SF2A 2007
J. Bouvier, A. Chalabaev, C. Charbonnel (eds)

FOURIER-DOMAIN WAVE-FRONT RECONSTRUCTION FOR LARGE ADAPTIVE OPTICAL SYSTEMS

C.Correia[1], J-M. Conan[1], C. Kulcsár[2], H-F. Raynaud[2], C. Petit[1] and T. Fusco[1]

Abstract. The astronomical community has now turned its attention to the development of adaptive optical systems (AOS) with a very large number of degrees-of-freedom (DoF), of which the new XAO (Extreme AO) and MOAO (Multi-Object AO) for Extremely Large Telescopes (ELT).

To tackle the wave-front reconstruction computational burden, spatial-frequency methods (FFTr) have been developed for systems featuring Shack-Hartmann wave-front sensors, which are considerably faster than standard vector-matrix multiplies (VMMr) and start being competitive in terms of performance.

We review their theoretical properties and the methods of *extension* and *circularization*, for which we propose new techniques. Applicability to open- and closed-loop systems is discussed by means of simulation results. Comparison with the VMM is presented to highlight their pros and cons.

1 Introduction

The wave-front reconstruction problem is at the front-line in the conception of AO systems for the future ELT. Larger apertures and even more complex high-resolution AOS amount at increasing substantially the DoF, whose feasibility relies on the possibility of reconstructing the wave-front from WFS data efficiently to avoid an insurmountable computational burden.

Wave-front reconstruction in the spatial-frequency (Fourier) domain is a long-stated problem, (Freischlad 1986), whose application to realistic AOS has however not been solved until the works of (Poyneer 2002, 2003), where the telescope's annular aperture is adapted to the squared-domain Discrete-Fourier Transform (DFT). Suitable use of the Fast Fourier Transform, a computational implementation of the DFT scaling as $O(nlog(n))$, with n the number of DoF, allows for the relaxation of the number-of-operations (NoO) of the so-far used reconstructors, which are based on matrix-vector multiplies, scaling as $O(n^2)$.

In this work we briefly outline the theoretical development of the underlying linear model and establish the conditions needed to comply with the DFT. We build on the Hudgin, (Hudgin 1977), and the Fried, (Fried 1977) approximate models focusing on the boundary constaints to adapt an annular to a squared aperture. We further develop the *full extension* for Fried geometry and the *apodized circularization* for the Hudgin geometry. A summary description of the regularized inverse filtering operators allowing to compute a command vector from SH-WFS measurements is provided. Final discussion is based on Monte-Carlo simulation results and on the assessment of effective costs to provide a comparison to the VMMr in terms of performance and suitability for real-time wave-front reconstruction.

Throughout this paper, small letters stand for direct-space whereas capital letters stand for spatial-frequency domain quantities/operators. Estimated quantities/operators have a tilde.

2 Direct Model

Two discrete measurement geometries have been proposed for the SH-WFS: the so-called Hudgin and Fried (Fig.1). We assume a discrete representation of the phase over a Cartesian grid of points. Both geometries approximate the discrete measurements by the first differences of the wave-front phase, which is an oversimplification of the true WFS measurements. Nonetheless, it presents features which make it suitable for wave-front

[1] Office National d'Etudes et de Recherches Aérospatiales, 29 Av. de la Division Leclerc, 92322 Châtillon.

[2] Laboratoire de Traitement et de Transport de l'Information, Univ. Paris XIII, 99 Av. Jean Baptiste Clément, 93430 Villetaneuse.

reconstruction on an annular-aperture. The measurement model for the Hudgin relates differences between contiguous points:

$$\begin{array}{ll} s_x\left[m,n\right] & = \phi\left[m,n+1\right] - \phi\left[m,n\right], \\ s_y\left[m,n\right] & = \phi\left[m+1,n\right] - \phi\left[m,n\right], \end{array} \tag{2.1}$$

whereas the Fried geometry averages differences between two parallel edges:

$$\begin{array}{ll} s_x[m,n] = & \frac{1}{2}\left(\phi\left[m,n+1\right] - \phi\left[m,n\right]\right) + \frac{1}{2}\left(\phi\left[m+1,n+1\right] - \phi\left[m+1,n\right]\right) \\ s_y[m,n] = & \frac{1}{2}\left(\phi\left[m+1,n\right] - \phi\left[m,n\right]\right) + \frac{1}{2}\left(\phi\left[m+1,n+1\right] - \phi\left[m,n+1\right]\right). \end{array} \tag{2.2}$$

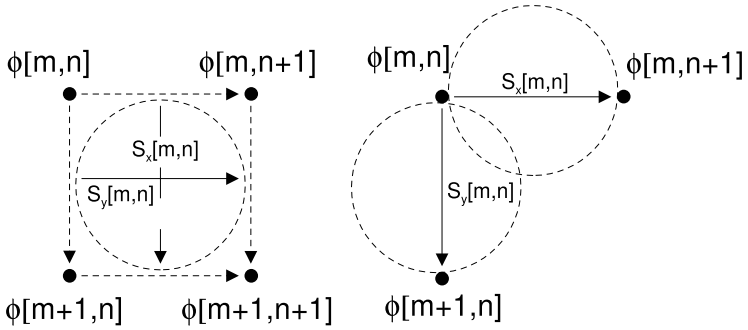

Fig. 1. Fried (left) and Hudgin (right) geometries that have been used as wave-front models.

2.1 Annular vs. squared apertures

The Fourier-domain reconstructor is based on the DFT, which is defined for a set of $N \times M$ points. In an AO case, due to the telescope aperture, the phase gradients are measured within an annular-aperture. To adapt them to the DFT algorithm, two constraints have been identified:

1. $rot(\nabla\phi) = 0$. Gradient field must be curl-free inside and outside the aperture.
2. The phase is assumed spatially periodic, due to the use of the N-point DFT. The integral of the gradient field over the $N \times N$-point DFT must be zero.

These two items are detailed in the next two sections.

2.1.1 Constraint 1): *Extension*

The *extension* relates to the application of constraint 1) in Sect. 2.1 to the discrete case: the sum of slopes in any closed-path must be zero, Eq. 2.3. A simple method of *extending* measurements outwards the aperture fully respects one such constraint. Figure 2 (left) details the procedure for the Hudgin geometry.

$$0 \quad = s_x[m,n] + s_y[m,n+1] - s_x[m,n+1] - s_y[m,n] \qquad 1 \le m \le N-1, 1 \le n \le N-1 \tag{2.3}$$

For the Fried geometry we have developed a new method of *extension*, which we called *full extension*. It is depicted in Fig. 2 (right). Our method aims at reconstructing the wave-front by using the slopes in the original x and y directions, in contradiction to the works of (Freischlad 1986) and (Poyneer 2002, 2003), in which the slopes are linearly recombined to form two rotated sets by doing $s_a[m,n] = -s_x[m,n] + s_y[m,n]$ and $s_b[m,n] = s_x[m,n] + s_y[m,n]$, further avoiding the reconstruction of two separated Hudgin-like problems. By employing this method and the corresponding inverse filter we are able to solve the reconstruction in much the same way as for the Hudgin geometry.

Since the Fried sensor provides the mean slope at the center of a sub-aperture, by averaging the phase difference at the corners (Eq.2.2), application of constraint 1) to the discrete case reads:

$$\begin{array}{ll} 0 \quad & = s_x[m,n] + s_x[m,n+1] + s_y[m,n+2] + s_y[m+1,n+2] \\ & \quad - s_x[m+2,n+1] - s_x[m+2,n] - s_y[m+1,n] - s_y[m,n], \quad 1 \le m \le N-2, 1 \le n \le N-2 \end{array} \tag{2.4}$$

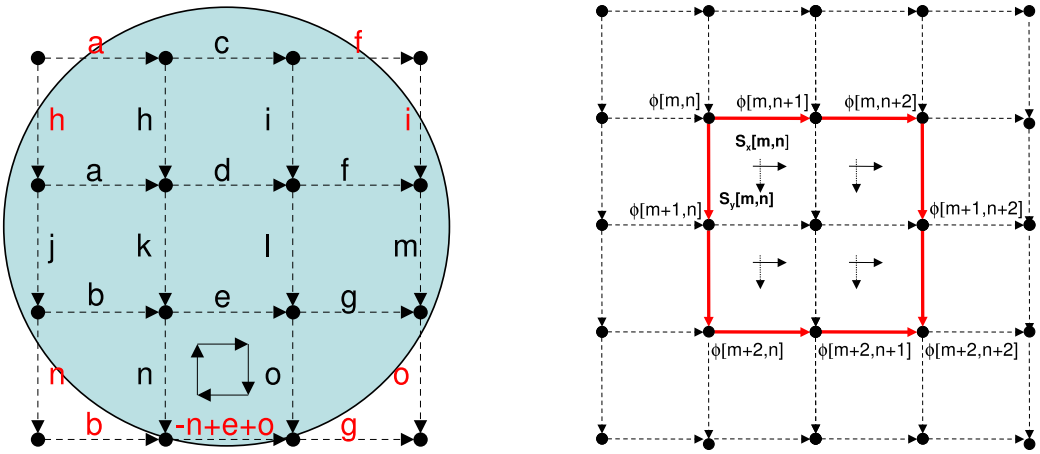

Fig. 2. Left: Hudgin *extension*. The measured slopes are represented in black letters, corresponding to sub-apertures within the aperture. The red slopes are *extended* outwards relating to the measured ones in the way shown. A special case that needs proper attention is the set of four neighbour corners for which only three slopes are measured. In this case the continuity constraints of phase applies, such that $\sum_{i=1}^{4} s_i = 0$, with s_i the slopes at the edges of the concerned sub-apertures; Right: Fried *full extension*. Any closed-path must be evaluated over the ensemble of four sub-apertures, following the slopes' directions and senses to closing up the path. The central point does not intervene in the computation. Only the slopes at the edges (full-red) of the four-tile sub-aperture are concerned.

2.1.2 Constraint 2): *Circularization*

Correct representation of the phase on the set of complex exponentials obliges circularizing the phase, for the basis set is periodic with period N.

The *circularization*, as proposed in (Freischlad 1986) and (Poyneer 2002, 2003) reads as

$$\sum_{n=1}^{N} s_x(m,n) = 0, \qquad \sum_{m=1}^{N} s_y(m,n) = 0. \tag{2.5}$$

It results that

$$\begin{aligned} s_x(m,N) &= -\sum_{n=1}^{N-1} s_x(m,n), \quad 1 \le m \le N \\ s_y(N,n) &= -\sum_{m=1}^{N-1} s_y(m,n), \quad 1 \le m \le N, \end{aligned} \tag{2.6}$$

providing an effective means to wrap-around the phase.

This method, though accurate, introduces slope jumps that translate into high-frequency components in Fourier space. We propose an improved *circularization* allowing for some degree of apodization. It consists of distributing the seam gradients of Eq.2.6 symmetrically across the aperture, according to a given apodizing function, in such way that Eq.2.5 still holds. Special conditions are imposed on the extended slopes, to fulfill both the constrains 1) and 2).

For the Fried geometry, imposition of constraint 2) affects constraint 1) at the edges of the support for an AO-like case. It will be accounted for as a reconstruction error.

3 Inverse Model

Using the shift property of the DFT, the estimate of the phase is obtained by inverting the Fourier-representation of measurement Eqs. 2.1-2.2 and solving for $\Phi[k,l]$:

$$\Phi_{Hudgin}[k,l] = \begin{cases} 0 & \text{if } k,l = 0; \\ \left\{\left[exp\left(-\frac{2\pi ik}{N}\right) - 1\right] S_x[k,l] + \left[exp\left(-\frac{2\pi il}{N}\right) - 1\right] S_y[k,l]\right\} \times \\ \left[4\left(sin^2\frac{\pi k}{N} + sin^2\frac{\pi l}{N}\right)\right]^{-1} & \text{otherwise.} \end{cases} \tag{3.1}$$

$$\Phi_{Fried}[k,l] = \begin{cases} 0 & \text{if } k,l = 0, N/2; \\ \{\left[exp\left(-\frac{2\pi ik}{N}\right)-1\right]\left[exp\left(-\frac{2\pi il}{N}\right)+1\right]S_x[k,l]+ & \\ \left[exp\left(-\frac{2\pi il}{N}\right)-1\right]\left[exp\left(-\frac{2\pi ik}{N}\right)+1\right]S_y[k,l]\}\times & \text{otherwise.} \\ \left[8\left(sin^2\frac{\pi k}{N}cos^2\frac{\pi l}{N}+sin^2\frac{\pi l}{N}cos^2\frac{\pi k}{N}\right)\right]^{-1} & \end{cases} \tag{3.2}$$

The filters can be written in the format $\tilde{\Phi} = \frac{G_x^* S_x + G_y^* S_y}{|G_x|^2+|G_y|^2}$. They both have a pole at the zero frequency, with the Fried being further blind to the waffle-frequency, (Poyneer 2002). This aspect is of crucial importance for the analysis that follows.

3.1 Regularized inversion

To smear the likely errors occurring at the higher-frequencies, we introduce a regularizing term relating to the noise and phase priors. Due to the *extension*, priors are not straightforward to estimate. We further introduce a factor γ that needs tuning to correctly weigh the priors. Following the derivation of the Wiener filter, application to the Hudgin and Fried geometries, which take into account the $x-$ and $y-$ slopes, has the form (frequency omitted)

$$\tilde{\Phi} = \frac{G_x^* S_x + G_y^* S_y}{|G_x|^2 + |G_y|^2 + \gamma\frac{W_n}{W_\phi}}, \tag{3.3}$$

where * is the complex-conjugate, W_n, $W_\phi \propto \mathbf{f}^{-11/3}$ the noise and phase power-spectrum density (PSD). For closed-loop simulations however, the term must be re-adapted to account for the temporal rejection of the closed-loop.

3.2 Deformable Mirror compensation

The wave-front estimate of Eq.3.3 relates to the actuator command through the convolution

$$\tilde{\phi} = a * h, \tag{3.4}$$

where a is the actuator command and h the deformable mirror (DM) influence function (IF) with the same spatial resolution as the phase resolution. The IF needs thus to be down-sampled to a coarser-grid resolution.

Since the convolution of Eq.3.4 becomes a multiplication in Fourier space, a simple operation applies. In order to avoid singularities and numerical misbehaviour, we introduce a regularization term

$$A = \frac{\tilde{\Phi}}{H + K}, \tag{3.5}$$

with K a bi-dimensional operator that penalizes a too large amplification of undesired frequencies.

4 Application to real-time systems

The whole interest of Fourier-methods relies on the reduced NoO. We extend the analysis, focusing instead on the number-of-operations per time-slot (computational performance is given in bits/second), which is of uttermost importance for the dimensioning of the real-time-computer (RTC). The total NoO is

$$NoO = 2\left(2\beta N^2 log_2(N) + 2N^2 + N^2 + \beta N^2 log_2(N)\right) + N^2 + 4N^2 \tag{4.1}$$

where the factor 2 is for the complex format, the first term for the forward FFT, the second the filter and the third the reverse FFT. Finally N^2 and $4N^2$ are for global and local waffle removal (Sec.3). Parameter $\beta \approx 5$ is a machine-dependent factor; N is the linear number of points considered for the bi-dimensional FFT. The *extension* and *circularization* are considered to have marginal costs and were thus disregarded.

Considering the VMM is partitioned in $N/2$ slots (slope computation is performed in $N/2$ elements, corresponding to two opposite stripes of WFS sub-apertures that are read-out per time-slot) - Fig. 3, we plot in Fig. 4 the scaling laws for the total NoO and the NoO performed in the last time-slot, which indeed is the one allocated for the whole computation of the FFTr (since it needs all the slopes prior to computation, it starts after the last slope computation). There are some arrangements allowing for some degree of optimization, but have not been considered in the present work.

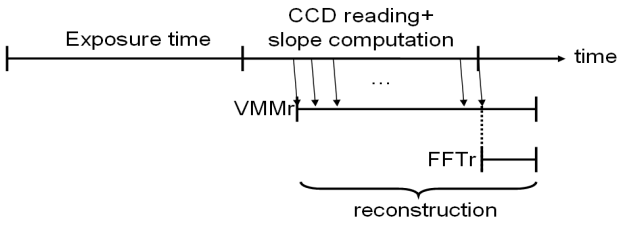

Fig. 3. Temporal arrangement of computations. VMM is partitioned in $N/2$ slots. The total RTC delay is given by the time taken to compute the last VMM portion.

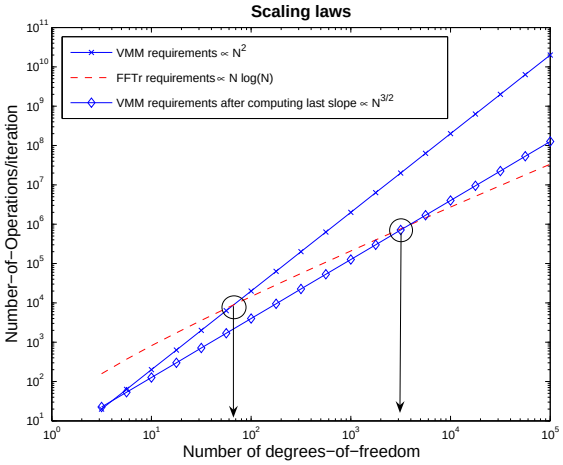

Fig. 4. Comparison of NoO for both the VMM and FFT vs. the number of degrees-of-freedom (full lines). The dashed line shows the amount of operations to execute in the last slot allocated to VMM, corresponding (apart from any other system particularity, as communication and data transport) to the total RTC delay. The FFTr used is a (N+2)-point two-dimensional FFT to accommodate the whole set of sub-apertures.

5 Monte-Carlo simulations

We have tested the FFTr in end-to-end Monte Carlo simulations, featuring a three-layer atmospheric profile $w_i = \{0.5, 0.2, 0.3\}, h_i = \{0, 1, 8\}km$ with a geometric 20×20 sub-aperture WFS and an integral controller with default gain $g = 0.4$ (for the closed-loop case). DM influence functions are Gaussian with 21% cross-coupling. Values of Strehl-ratio shown in percentage were computed at $\lambda_{WFS} = 2.2\mu m$, for a seing of $0.65''$. Phase-screens are generated at high resolution (10×10 pixels/sub-aperture) and deal correctly with low-frequencies. VMM reconstructor consists of the generalized inverse of the interaction matrix, obtained through truncated singular-value-decomposition.

Open-loop simulations show the gains brought by regularizing and imposing the correct constraints on the *extension* procedure. Results are summarized in Table 1. The use of the Hudgin geometry in open-loop simulations is substantially worst than the Fried geometry. In contrast with the latter, regularizing and apodizing the *circularization* is of marginal interest. This so happens because regularization attempts at penalizing frequencies corresponding to pole locations. Hugdin's inverse filter single pole is located at the zero-frequency (piston). The remaining of the discrete-frequencies can be accurately reconstructed, being the regularization of no practical influence. When compared to the Fried, Hudgin is less descriptive of the SH-WFS, behaving poorer by $3 - 4\%$.

As for the Fried case there is a clear advantage of using correctly extended slopes with respect to simply extending slopes outwards. Regularization provides $\approx 2\%$ increase in Strehl-ratio. The loss for the reference

VMMr case is $< 3\%$.

Table 1. Open-loop results. Strehl-ratio (percentage) evaluated at $\lambda_{WFS} = 2.2\mu m$. Seeing $0.65''$ for a bright star of $m_v = 8$. For the Hudgin geometry we compare the *normal* with the *apodized circularization*, whereas for the Fried case we compare the effects of using the *full extension*. For both cases, the impact of regularizing is shown.

		Normal circularization	**Apodized circularization**
Hudgin	**Regularized**	79.33± 4.38	79.42 ± 4.25
	Non-regularized	79.25 ±4.39	79.37 ± 4.31
		Full extension	**Simple extension**
Fried	**Regularized**	83.32 ± 3.1	82.25 ± 3.53
	Non-regularized	81.27 ± 2.55	80.76 ± 3.02
VMM		85.90	

We further tested scenarios of stronger turbulence for which regularization becomes all the more important.

In closed-loop simulations, however, the Hudgin geometry behaves better than the Fried, though it models more crudely the WFS. Badly-seen modes (of which the waffle and local waffle) are not damped by the integrator loop, requiring further filtering. The introduction of an extra regularizing function to tailor the system to correct behaviour is able to stabilize the Strehl-ratio, but at levels that are not yet satisfactory, since the relatively large errors obtained located at the aperture's edge sacrifice the performance.

6 Discussion

Fourier-reconstruction for AOS is still a premature technique. Though great developments and abundance of filtering options, they present an average lower performance in terms of Strehl-ratio than its VVMr counterpart. Several reasons are in order: direct-problem modelling is too severe in the assumptions made; imposition of constraints on the extended phase do not hold in the presence of noise; DM modelling assumes influence-functions are translation-invariant.

Nonetheless, performance attained by the FFTr is substantially improved by the use of both the regularization and the *full extension* for the case of Fried geometry. Regularization becomes even more influential for dimmer stellar objects.

Computational-costs are indeed very attractive. FFTr decreases considerably the total effort when compared to the VMMr. We introduced the arrangement of computations during the iteration elapsed-time. For ELT great diminishment of the NoO is expected. Real-time requirements decrease for systems featuring more than ≈ 3000 DoF, although the NoO is equivalent for a system with as few as ≈ 70 DoF. For simulations, the latter is the value one needs to retain.

A primordial question subsists: Are the real-time constraints so restrictive so as to deploy cost-effective sub-optimal algorithms instead of improving optimal algorithms to meet real-time requirements? Future work by the authors on these issues will attempt at delivering some answers.

We would like to thank Laurent Mugnier for numerous exchanges on the development of the FFTr.

References

Hudgin, R. 1977, Journal of the Optical Society of America, 67, 375-378

Freischlad, K. R., & Koliopoulos, C. L. 1986, Optical Society of America Journal A, 3, 1852-1861

Fried, D. L. 1977, Journal of the Optical Society of America (1917-1983), 67, 370-375

Poyneer, L. A., Gavel, D. T., & Brase, J. M. 2002, Optical Society of America Journal A, 19, 2100-2111

Poyneer, L. A. 2003, Advanced techniques for Fourier transform wavefront reconstruction, ed. Peter L. Wizinowich & Domenico Bonaccini, 4839, 1023-1034